Biomaterials 32 (2011) 6068–6079

Contents lists available at ScienceDirect

Biomaterials

journal homepage: www.elsevier.com/locate/biomaterials

Robust CNS regeneration after complete spinal cord transection using aligned poly-L-lactic acid microfibers

Andres Hurtado [a,b,*,1], Jared M. Cregg [a,c,1], Han B. Wang [c], Dane F. Wendell [a], Martin Oudega [d], Ryan J. Gilbert [c,2], John W. McDonald [a,b,e]

[a] International Center for Spinal Cord Injury, Hugo W. Moser Research Institute at Kennedy Krieger, Baltimore, MD 21205, USA
[b] Department of Neurology, Johns Hopkins University, Baltimore, MD 21205, USA
[c] Department of Biomedical Engineering, Michigan Technological University, Houghton, MI 49931, USA
[d] Departments of Physical Medicine & Rehabilitation, Neurobiology, and Biomedical Engineering, University of Pittsburgh School of Medicine, Pittsburgh, PA 15213, USA
[e] Department of Physical Medicine & Rehabilitation, Johns Hopkins University, Baltimore, MD 21205, USA

ARTICLE INFO

Article history:
Received 14 April 2011
Accepted 1 May 2011
Available online 1 June 2011

Keywords:
Spinal cord injury
Axonal regeneration
Axon guidance
Polylactic acid
Electrospinning
Aligned microfibers

ABSTRACT

Following spinal cord injury, axons fail to regenerate without exogenous intervention. In this study we report that aligned microfiber-based grafts foster robust regeneration of vascularized CNS tissue. Film, random, and aligned microfiber-based conduits were grafted into a 3 mm thoracic rat spinal cord gap created by complete transection. Over the course of 4 weeks, microtopography presented by aligned or random poly-L-lactic acid microfibers facilitated infiltration of host tissue, and the initial 3 mm gap was closed by endogenous cell populations. This bulk tissue response was composed of regenerating axons accompanied by morphologically aligned astrocytes. Aligned fibers promoted long distance (2055 ± 150 μm), rostrocaudal axonal regeneration, significantly greater than random fiber (1162 ± 87 μm) and film (413 ± 199 μm) controls. Retrograde tracing indicated that regenerating axons originated from propriospinal neurons of the rostral spinal cord, and supraspinal neurons of the reticular formation, red nucleus, raphe and vestibular nuclei. Our findings outline a form of regeneration within the central nervous system that holds important implications for regeneration biology.

1. Introduction

Axons fail to regenerate spontaneously after CNS injury [1,2]. Regeneration failure can be partially attributed to a limited intrinsic axon growth capacity of adult neurons [3,4]. Indeed, augmenting the growth potential of centrally projecting axons via peripheral conditioning or other cAMP-dependent mechanisms improves axonal regeneration [2,5–7]. Likewise, delivery of neurotrophins results in comparable gains [8,9]. In addition to a limited growth capacity, an inhospitable extracellular environment hinders regeneration. Moderate microtubule stabilization increases the regeneration ability of axons while mitigating the inhibitory properties of scar tissue [3]. Other therapeutic interventions that neutralize inhibitors associated with residual myelin [10–12] or chondroitin-sulfate proteoglycan [12–14], a scar-associated inhibitor, also lead to improvements in axonal regeneration. Despite observations of modest gains (~500 μm) using pharmacological therapies, neurons within the CNS can achieve long distance axonal regeneration.

After Richardson et al. [15] revived work performed by Ramón y Cajal and demonstrated the ability of CNS axons to regenerate into PNS grafts, several groups have observed long distance regeneration using this approach [16–18]. Within peripheral nerve grafts, parallel columns of Schwann cells surrounded by basal lamina (bands of Büngner) render excellent guidance to regenerating axons. However, harvesting autografts is limited by tissue availability and donor site morbidity, and the alternative acellularized allografts fail to support axonal regeneration [19,20]. To mimic the favorable attributes of peripheral nerve grafts, several groups have used Schwann cells and topographic/chemotropic guidance cues to support regeneration [7,21–25]. Nevertheless, poor survival [24] limits the potential of cellular therapies, and neurotrophin administration requires precise timing, dose, and spatial distribution [26].

* Corresponding author. International Center for Spinal Cord Injury, Hugo W. Moser Research Institute at Kennedy Krieger, 707 N Broadway, Suite 523, Baltimore, MD 21205, USA. Tel.: +1 443 923 9248; fax: +1 443 923 9245.
E-mail address: hurtado@kennedykrieger.org (A. Hurtado).
[1] Andres Hurtado and Jared M. Cregg contributed equally to this work.
[2] Present address: Department of Biomedical Engineering, Rensselaer Polytechnic Institute, Troy, NY 12180, USA.

0142-9612/$ – see front matter © 2011 Elsevier Ltd. All rights reserved.
doi:10.1016/j.biomaterials.2011.05.006

Spinal cord injury often results in substantial loss of neural tissue [27]. Several groups are investigating tissue engineering approaches to bridge large spinal cord gaps. Recent advances in biomaterials engineering have provided a potential synthetic platform for neural regeneration. Electrospun fibers have garnered attention for their ability to guide neurite growth [28–30] and promote regeneration across long peripheral nerve gaps [30–32]. In the present work we hypothesized that topographic cues provided by aligned poly-L-lactic acid (PLA) microfibers would promote axonal regeneration within the CNS. We report the effects of implanting biodegradable conduits with aligned microfibers in an acute complete transection rat model of spinal cord injury.

2. Materials and methods

2.1. Materials fabrication

2.1.1. Solution casting PLA films

Glass coverslips (15x15 mm; Proscitech, Australia) were coated with a thin PLA (NatureWorksTM, grade 6201D, Lot #9051-89-2, density: 1.25, weight average: MW 78 kDa, number average: MW 48 kDa, Cargill Dow LCC, Minnetonka, MN) film by solution casting a 4% w/w polymer solution of PLA dissolved in a 1:1 dichloromethane:chloroform organic solvent mixture.

2.1.2. Electrospinning PLA fibers onto films

PLA fibers were obtained by electrospinning an 8% w/w polymer solution of PLA/solvent as previously described [28]. In brief, PLA solution was loaded into a glass syringe and delivered for 45 min at a rate of 1.5 ml/h. Coverslips coated with thin PLA films were secured to a grounded aluminum collector disc. A 15 kV potential was used to electrospin the PLA solution onto a stationary target to generate random fibers, or a target rotating at 1500 rpm to generate aligned fibers (Fig. 1A,B). Coverslips with fibers were placed into a fume hood overnight at room temperature to evaporate residual solvent. At this point samples for in vitro experiments were sterilized using an ethylene oxide sterilizer (An74i, Anderson Products, Inc. Haw River, NC) for a 12 h cycle.

2.1.3. Conduit assembly

PLA films (with or without electrospun fibers) were peeled from coverslips (Fig. 1C) for conduit assembly. Two specimens of the same type were placed back-to-back and rolled into conduits (Fig. 1D–F). A middle insert (Fig. 1F,N) was created within the conduit lumen to increase the surface area for cell–substrate interaction [32] and to decrease the probability of tube collapse [22]. Prior to in vivo experiments samples were sterilized using an ethylene oxide sterilizer for a 12 h cycle.

2.1.4. Materials characterization

Alignment of polymeric fibers was assessed in scanning electron microscopy (SEM) micrographs before and after conduit assembly using previously described methods [28,30]. Specimens were coated with gold (5 nm) by sputter deposition and micrograph images were taken using a Hitachi S-4700 FESEM. Fiber alignment was quantified by measuring the angle between a given fiber and the median fiber orientation. Angle difference was recorded for fifty fibers from each of 3 independently fabricated specimens (total of 150 fibers per condition) as previously described [28].

2.2. Cell culture

2.2.1. Dorsal root ganglia culture

All animal procedures were conducted in accordance with protocols approved by the Institutional Animal Care and Use Committee (IACUC) at The Johns Hopkins University. DRG were isolated from P4 Sprague-Dawley rat pups [30]. After removing the roots, ganglia were split into halves and explants were cultured on film, random, or aligned fiber specimens for 5 days in neurobasal media with B-27 and nerve growth factor (50 ng/ml). Adult DRG were isolated from 16 week old rats and incubated for 90 min in collagenase (200 U/ml) and dispase (4 U/ml). After washing several times with HBSS, dissociated neurons were plated on poly-L-lysine (100 μg/ml) and laminin (10 μg/ml) coated film, random, or aligned fiber specimens at a density of 7,500 cells/cm^2 and maintained in neurobasal media with B-27 for 5 days.

2.2.2. Astrocyte culture and migration assay

Astrocytes were isolated from E18 Sprague-Dawley rat pups [33]. Cerebral cortices were isolated, meninges removed, and tissue was treated with 0.01% trypsin and mechanically dissociated by trituration through a Pasteur pipette. Cells were then plated on poly-D-lysine (10 μg/ml) coated flasks, and maintained in culture for 10 days. Cultures were purified for astrocytes by vigorous shaking to remove non-adherent cells. For morphological characterization, astrocytes were plated onto poly-D-lysine (10 μg/ml) coated film, random, or aligned fiber specimens at a density of 4000 cells/cm^2 and maintained for 48 h in culture in DMEM with 10% FBS. Cell culture inserts with two wells (12.5 mm by 5 mm each) separated by a distance of 2.25 mm were used for an astrocyte migration assay similar to a meningeal cell migration assay described previously [3]. A total of 50,000 cells were plated in each well to obtain a confluent layer, and astrocytes were allowed to attach for 24 h. At 24 h, the chambers were removed and the specimens (film, random, or aligned fibers) were washed once to remove non-adherent cells. Three ($n = 3$) samples from each group were immediately fixed ($t = 0$), and 30 additional specimens ($n = 10$ per group) were maintained in culture in DMEM with 10% FBS for 5 additional days.

2.2.3. Cortical explants

Cortical explants were isolated from E18 rat pup cortices. Cerebral cortices were harvested and a Pasteur pipette was used to punch relatively uniform tissue explants from cortices. Explants were then cultured on film, random, or aligned fiber substrates ($n = 8$ per group) for 5 days in neurobasal medium with 5% FBS.

2.2.4. Immunocytochemistry

Cells were fixed for 1 h in 4% PFA and blocked for 1 h in PBS/10% normal goat serum (Sigma–Aldrich) and 0.4% triton-X (Sigma–Aldrich). DRG were incubated overnight at 4 °C with chicken anti-neurofilament (NF, 1:1000; Millipore, Temecula, CA), astrocyte cultures with rabbit anti-GFAP (1:1000; Dako, Carpinteria, CA), and cortical explants with both anti-NF and anti-GFAP primary antibodies. Specimens were subsequently incubated for 1 h with goat anti-chicken Alexa-488/546 or goat anti-rabbit Alexa-488/680 conjugated secondary antibodies. Cells were counterstained with Hoechst (H, 1:2000) and specimens were mounted on glass slides for imaging using either an Olympus BX61 upright fluorescence microscope or an Olympus Fluoview FV1000 confocal microscope.

2.2.5. Quantitative analysis

Neurite extension was analyzed by separately fitting DRG explants ($N = 18$; $n = 6$ per group) and fields of neurite extension from fluorescent neurofilament images to an elliptical model using least-squares regression [34,35]. From these images, eccentricity and maximum/average neurite distance were calculated. Eccentricity was used as a measure of anisotropy where 0 (in the case of a perfect circle) represents no preferential direction of neurite extension and 1 (in the case of straight line) represents perfect directionality.

Astrocyte migration was assessed on film, random, and aligned fiber substrates by measuring the distance between migration fronts at 10 points separated by 1.25 mm (along the 12.5 mm fronts); these 10 measurements were pooled to calculate the sample mean. Group means were calculated by averaging sample means ($t = 0$, $n = 3$; $t = 5$ d, $n = 10$). After 24 h in culture and immediately after chamber removal, 3 samples from each group (film, random, aligned) were fixed and stained to measure initial separation distance. Data are presented as migration distance which represents the separation distance at 5 days after chamber removal (mean ± SEM) from ten different samples ($N = 30$; $n = 10$ per group) subtracted from the initial separation distance.

2.3. Complete transection model of spinal cord injury

2.3.1. Animals

Female Sprague–Dawley rats ($N = 45$, 250 g; Harlan, Indianapolis, IN) were housed according to NIH and USDA guidelines. The IACUC of Johns Hopkins University approved all animal procedures. Rats were randomly divided into 3 groups (film, $n = 13$; random, $n = 13$; aligned fiber, $n = 19$) and were euthanized at 1 ($n = 9$, 3 per group), 2 ($n = 9$, 3 per group), and 4 ($n = 27$, 7 film, 7 random and 13 aligned) weeks after conduit implantation. Importantly, the data for the 4 week time point was acquired in two separate experiments. A third group of animals ($n = 6$) with aligned fibers conduits was used for retrograde tracing.

2.3.2. Conduit implantation

Rats were anesthetized with an intramuscular injection of 60 mg/kg ketamine and 0.4 mg/kg metidomidine. Animal backs were shaved and aseptically prepared, and ophthalmic ointment (Lacrilube; Allergen Pharmaceuticals, Irvine, CA) was applied. Spinal cord complete transection and conduit implantation were performed as described previously [24]. After opening the skin and muscle layers, a dorsal laminectomy (Supplementary Fig. 1A) was performed on the thoracic eight (T8) vertebra and the dura mater was carefully opened. The exposed T9-10 spinal cord was transected using angled scissors; a first cut was made at the rostral end of the laminectomy (Supplementary Fig. 1B) and then 1–2 mm of tissue were completely removed creating a 3 mm gap (Supplementary Fig. 1C). After hemostasis was achieved, a 3 mm long conduit (film, random, or aligned fiber) was implanted to bridge the gap between the rostral and caudal spinal cord stumps (Supplementary Fig. 1D). Prior to implantation, all conduits were filled with a solution of 1% fibrinogen (Type 1, human plasma; Sigma–Aldrich) in DMEM with 2% $CaCl_2$, 2% aprotinin (Sigma–Aldrich), and 0.2% gentamicin (Gibco). After conduit implantation, a layer of silicone sheeting (0.005" thick) was placed over the implant and both cord stumps. Muscle layers were sutured and the skin was closed

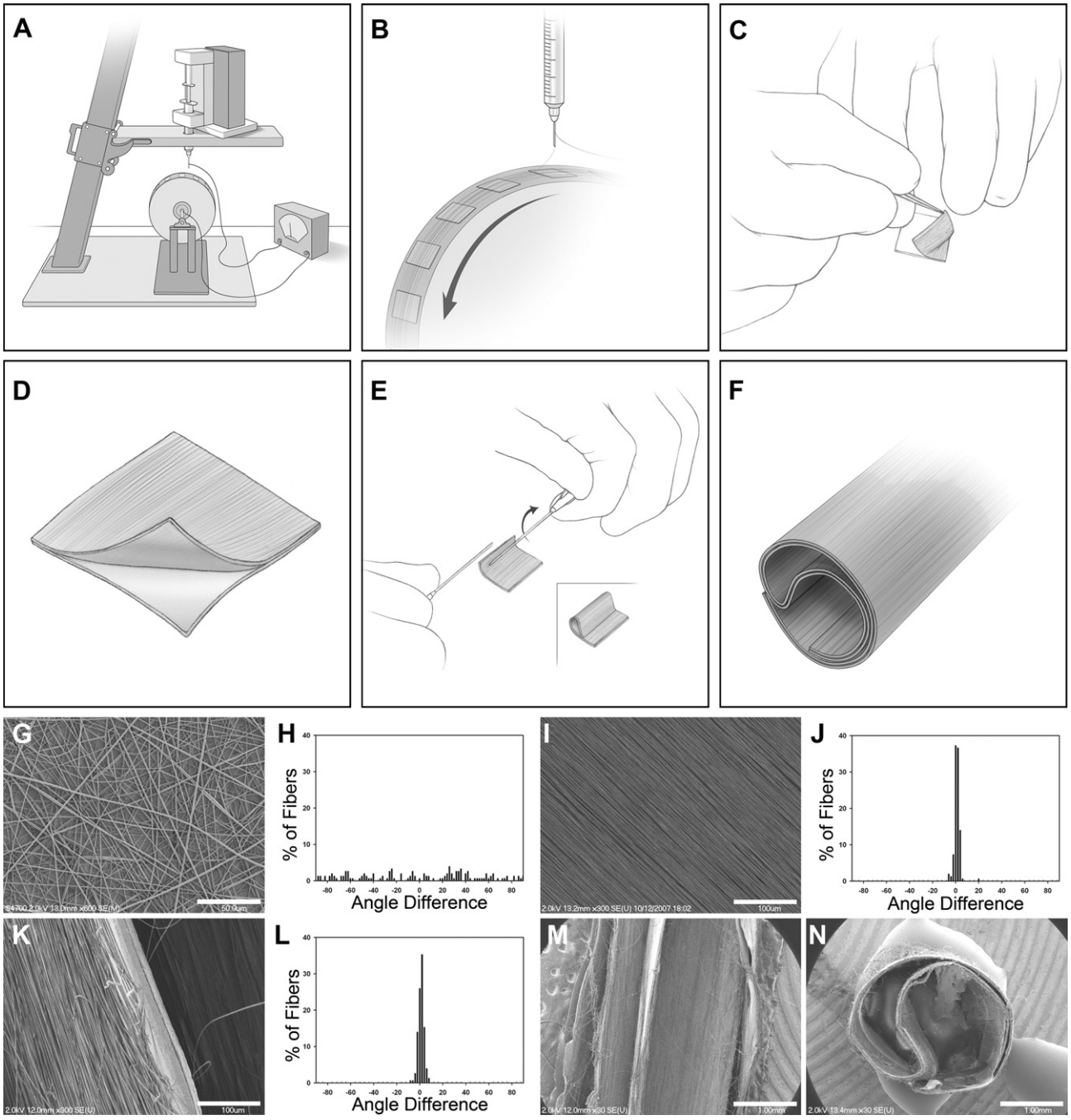

Fig. 1. Schematic detailing materials fabrication process and materials characterization. A custom electrospinning apparatus (A) was used to generate aligned polymeric fibers. Coverslips were mounted on a grounded target, and a rotation speed of 1500 rpm was used to align fibers produced by a 15 kV field potential (B). Random fibers were generated using a stationary target. For conduit assembly, films with or without electrospun fibers were peeled from coverslips (C), placed back to back (D), and rolled (E) into conduits (F). Random (G) and aligned (I) fibers were visualized by scanning electron microscopy, and alignment was quantified by measuring the angle between a given fiber and the median fiber orientation for 150 fibers per condition (H and J, respectively). Importantly, fiber alignment was maintained through the process of conduit assembly (K and L). (M) Macroscopic view of aligned fiber conduit lumen, visualized by mounting a conduit sectioned on the longitudinal axis. (N) Coronal view of an aligned fiber conduit, the diameter of all conduits was 2.6 mm. Scale bars: 50 μm in (G); 100 μm in (I and K); 1 mm in (M and N).

with metal wound clips. During surgery, rats were kept on a heating pad to maintain body temperature. Immediately after surgery, rats received 10 ml of warm (37 °C) Ringers' solution subcutaneously and 0.03 ml of gentamicin (40 mg/ml; Buck, Inc., Owings Mills, MO) intramuscularly. Anesthesia was reversed with an IM injection of 0.05 ml (1 mg/kg) atipamezole hydrochloride (Antisedan®; Pfizer Animal Health, Exton, PA). All animals were allowed to recover from anesthesia in a small animal incubator set at 30 °C. After full recovery, rats were returned to their cages with *ad libitum* water and food. Gentamicin (0.03 ml) was administered IM daily for seven days to prevent urinary tract infection. Bladders were expressed manually twice a day until reflex bladder voiding returned. Throughout further survival, bladders as well as general health of the rats were monitored at least once a day. In cases of urinary tract infection, gentamicin administration was reinitiated for 7-10 days.

2.3.3. Assessment of hindlimb motor function

In rats that survived for 4 weeks, changes in hindlimb function were assessed using the test developed by Basso, Beattie, and Bresnahan [36,37], an open field test with a 22-point scale (0 represents no movement of hindlimbs and 21 represents normal locomotion). During the week before surgery, rats were tested twice to become accustomed to the testing environment. During survival after surgery, rats

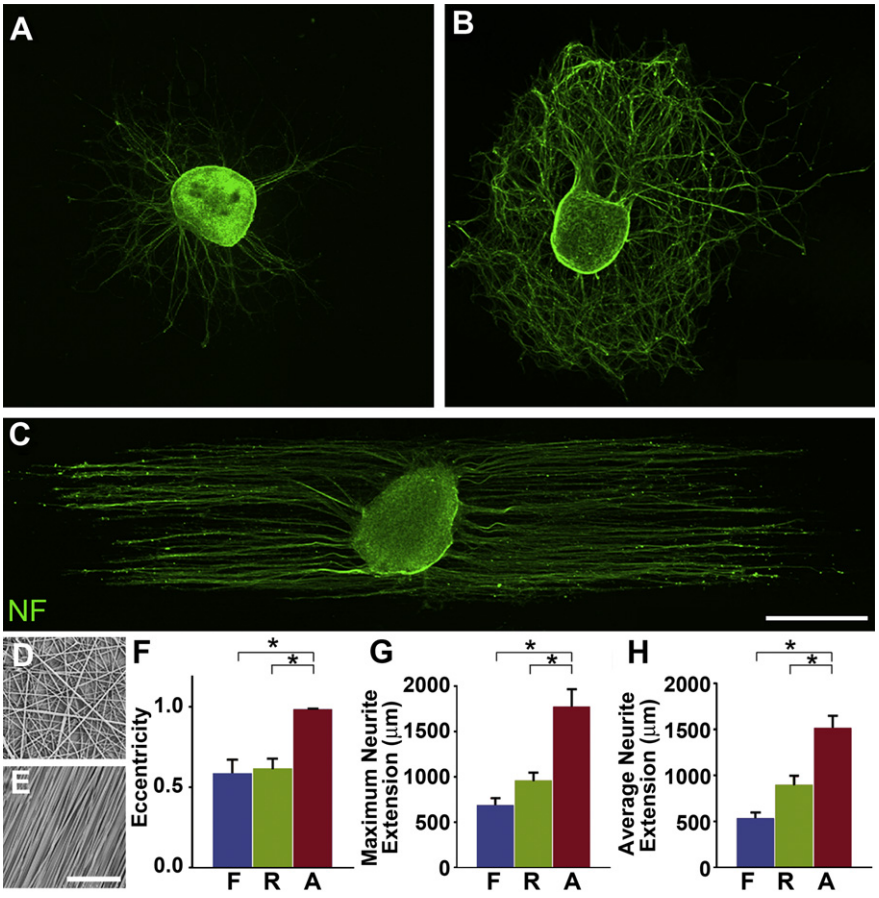

Fig. 2. Aligned polymer fibers specify the direction of DRG neurite growth. DRG isolated from P4 rat pups were cultured on film (A), random (B), and aligned fiber (C) substrates. Random (D) and aligned (E) polymer fibers were characterized by scanning electron microscopy. The eccentricity (F), a measure of anisotropy, and the maximum (G) and average (H) distance reached by neurites were quantified on DRG explants. Markedly, aligned polymer fibers elicited linear neurite elongation, providing an efficient means of growth as demonstrated by a significant increase in the maximum and average distance reached by neurites over the same time in culture. F, film; R, random; A, aligned. Data are mean ± SEM; $n = 6$. *$P < 0.05$ by ANOVA. Scale bars: A-C, 500 μm; D, E, 50 μm.

were tested once a week for 4 min by two independent observers who were oblivious to the experimental paradigms.

2.3.4. Retrograde axonal tracing

Four weeks after injury and conduit implantation rats were anesthetized and prepared for surgery as above. Scar tissue was gently removed and the implanted conduit was re-exposed. A midline longitudinal incision through the dorsal surface of the conduit was made using angled microscissors (Fine Science Tools, Foster City, CA) exposing the regenerated tissue underneath. Using a glass needle attached to a 1 μl Hamilton syringe, 0.5 μl of Fast blue were injected 1.5 mm caudal to the rostral end of the conduit at a rate of 0.25 μl/min. The needle was left in place for an additional 2 min to avoid tracer leakage and then slowly withdrawn [24]. Muscle layers were sutured, the skin was closed with metal wound clips, and animals received postoperative care as above. Rats were perfused (see below) 7 days later.

2.3.5. Tissue preparation and immunohistochemistry

One, two, and four weeks after conduit implantation, rats were anaesthetized as above. After deep anesthesia was confirmed, the heart was exposed and 500 IU of Heparin (Henry Schein, Melville, NY) was injected into the left ventricle. Next, 300 ml of 1x PBS followed by 300 ml ice-cold 4% PFA in 1x PBS was perfused through the vascular system. Spinal cords were removed and post-fixed overnight at 4 °C in the same fixative. A 15 mm long segment centered on the conduit and including the rostral and caudal spinal cord stumps as well as a 10 mm segment including the brainstem were dissected and transferred to phosphate-buffered 30% sucrose (Supplementary Fig. 1E,F show dissected conduits 1 and 4 weeks after implantation, respectively). After 48 h, tissue was frozen within shandon M-1 embedding matrix (Thermo Electron Corporation, Pittsburgh, PA). From these spinal cords, 20 μm thick horizontal sections were cut on a cryostat, mounted onto glass slides, and stored at −20 °C. Brainstems were cut into 40 μm thick coronal sections, mounted onto glass slides and stored at −20 °C. Spinal cord cryostat sections were permeabilized with 0.3% Triton X-100 in PB (0.1 M, pH 7.4), immuno-blocked with 5% normal goat serum in PB at room temperature for 30 min, and then immunostained as previously described [24]. The following primary antibodies were used: rabbit antibodies against glial fibrillary acidic protein (GFAP, 1:200; Incstar Corp., Stillwater, MN), serotonin (5HT, 1:200; Immunostar, Hudson, WI) and laminin (LAM, 1:400; Sigma–Aldrich). Mouse antibodies were directed against neurofilament (RT97, 1:5; Developmental Studies Hybridoma Bank) and rat endothelial cell antigen (RECA-1, 1:25; Serotec). Stained sections were coverslipped using Vectashield/DAPI (Vector Laboratories, Inc., Burlingame, CA) and kept at 4 °C until analysis. Adjacent sections were stained using cresyl violet. Images were taken on either an inverted Olympus IX70 microscope or an Olympus Fluoview 1000 confocal system at an original magnification of 20× with individual filter sets for each channel, and were assembled using Adobe Photoshop CS5.

2.3.6. Quantitative tissue analysis

Tissue volume was assessed in the cresyl violet stained sections using the Cavalieri estimator probe (grid spacing: 250 μm) from StereoInvestigator® (MBF Bioscience, Williston, VT). From each animal, every tenth cryostat section (200 μm intervals) was used to determine the volume of tissue inside the conduit; tissue volume is expressed as the percentage of conduit lumen containing Nissl stained cell bodies. The distance between the rostral edge of the conduit to the 'axonal front', defined as the point at which there is a group of 10 or more contiguous fibers, was quantified at all time points in the RT97/GFAP-stained sections [38]. At the 4 weeks time point, the number of animals that had grown CNS tissue (defined by presence of RT97 and GFAP inside the conduit) was quantified at the rostral graft interface and every 500 μm in the rostrocaudal direction. Fast Blue labeled neurons were counted on every sixth 40 μm-thick coronal section throughout the brainstem. Sections were scanned at 20x and all cells were counted after morphological confirmation under 40× magnification.

2.4. Statistical analysis

JMP IN software (Release 7.0.2; SAS, Cary, NC) was used to carry out all statistical analyses. A one-way ANOVA test was performed to determine statistical differences

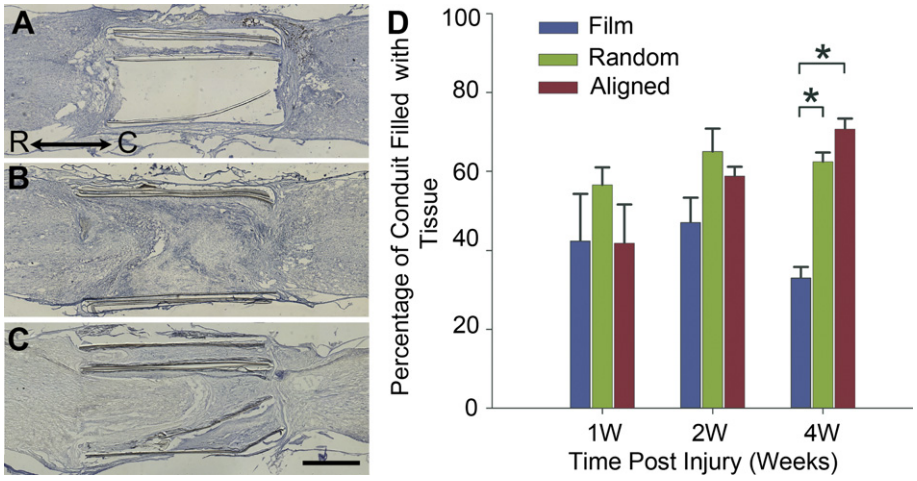

Fig. 3. Microtopography promotes host tissue integration and gap closure. A 3 mm long conduit was implanted to bridge a complete transection spinal cord injury. Cresyl violet was used to visualize tissue architecture. Representative images 4 weeks after implantation of film (A), random (B), and aligned fiber (C) conduits demonstrate that both random and aligned fibers support tissue integration into conduits and limited cavitation in host cord tissue. A Cavalieri estimator probe was used to measure tissue volume inside conduits at 1, 2, and 4 weeks post injury (D). Both random and aligned fiber conduits had significantly more endogenous tissue than film conduits at 4 weeks. Data are mean ± SEM; $n = 3$ (1W, 2W), $n = 7$ (4W). *$P < 0.05$ by ANOVA. Scale bar: A-C, 1 mm.

between groups for eccentricity, maximum neurite length, average neurite length, percentage of conduit filled with tissue, average rostrocaudal axonal regeneration, and migration distance. If groups were statistically different in the ANOVA test, a post-hoc Tukey–Kramer HSD test was used to compare all pairs individually. Repeated measures ANOVA was used to determine whether differences between groups mean hindlimb BBB scores were statistically significant. $P < 0.05$ was considered to be statistically significant. All data are presented as mean ± SEM.

3. Results

3.1. Neurite growth from dorsal root ganglia

Polymer microfiber substrates were fabricated by electrospinning an 8% PLA solution onto 20 μm thick PLA films (Fig. 1) [28]. Randomly oriented fibers were deposited on films (Fig. 1G) by electrospinning PLA onto a stationary target; a rotating target was used to make aligned fiber substrates (Fig. 1I) as described in our previous work [28]. Fiber diameter and alignment were analyzed from scanning electron micrographs (Fig. 1G,I and Fig. 2D,E). Fiber diameter ranged between 1.2 and 1.6 μm. Only 4% of random fibers were found to fall within ± 4° of the median fiber orientation (Fig. 1H), whereas 97.3% of aligned fibers fell within ± 4° of the median orientation (Fig. 1J).

Dorsal root ganglia (DRG) isolated from P4 rat pups were cultured on film, random, and aligned fiber substrates for 5 days in serum free media ($n = 6$ per condition). DRG cultured on film and random fiber substrates projected neurites without preferential direction (Fig. 2A,B). However, in the presence of aligned PLA fibers, DRG projected linear neurites following the polymer microfiber orientation (Fig. 2C). Explants cultured on aligned PLA microfibers demonstrated a significant increase in eccentricity, a measure of anisotropy (Fig. 2F). Neurites from DRG cultured on aligned fibers reached significantly greater maximum and average distances compared with random fiber and film controls ($P < 0.05$) (Fig. 2G, H). We explored whether topography alone (regardless of orientation) can induce a differential response from DRG neurons. Neurites of DRG cultured on random fibers (Fig. 2B) were more dense than those of DRG cultured on films (Fig. 2A); however, the average and maximum distance reached by neurites was similar under both conditions (Fig. 2G,H). Dissociated adult DRG neurons also align their axons to the underlying topography (Supplementary Fig. 2C), suggesting that this phenomenon is independent of developmental stage.

3.2. Host tissue integration

Guidance conduits were fabricated by rolling film, random, and aligned fiber 2D substrates into conduits (Fig. 1C–F,N). Importantly, conduit fabrication did not perturb fiber alignment; 93.3% of fibers fell within ± 4° of the median orientation post-fabrication (Fig. 1L). An unambiguous, complete transection model of rat spinal cord injury was used to test the hypothesis that aligned microfibers promote axonal regeneration after CNS injury. A 3 mm gap was created in the spinal cord (thoracic 9) of adult rats, and immediately after, film, random, or aligned fiber conduits filled with a fibrin gel were grafted into the gap (Supplementary Fig. 1). Animals from each group were perfused 1 ($n = 3$), 2 ($n = 3$), and 4 weeks ($n = 7$) following injury/implantation. The results from the 4 week time point were gathered in two independent experiments of $n = 3$ and $n = 4$ for each group.

Cresyl violet and DAPI staining were used to assess cytoarchitecture in horizontal spinal cord sections. One week after transplantation remnants of the fibrin gel were present inside conduits and host cells had infiltrated the conduits' lumen (Supplementary Fig. 3A–C). Cell population increased substantially by two weeks in all groups (Supplementary Fig. 3D–F); however, at this time point film conduits started to show a decrease in transverse diameter of the lumen content (Supplementary Fig. 3D). By 4 weeks (Fig. 3 and Supplementary Fig. 3G–L), film conduits presented thin tissue strands and large (>1 mm diameter) cavities had developed at the rostral (2/7 animals) and caudal (4/7 animals) graft-cord interfaces (Fig. 3A). In contrast, conduits with random or aligned microfibers promoted tissue sparing at both interfaces, where 1 out of 14 animals with either random or aligned fiber conduits had a cavity in the caudal spinal cord at 4 weeks. Additionally, random and aligned fiber conduits were filled with host tissue at 4 weeks after implantation and the initial 3 mm tissue gaps were closed by endogenous cell populations (Fig. 3B,C and Supplementary Fig. 3H,I,K,L). One remarkable observation was the tissue continuity at the rostral interface of random and aligned fiber conduits (Fig. 3B,C and Supplementary Fig. 3H,I). In contrast, a scar-like matrix developed at both interfaces of film conduits, and

exclusively at the caudal interface of random and aligned fiber conduits (Fig. 3B,C and Supplementary Fig. 3H,I). A Cavalieri estimator probe was used to quantify the percentage of conduit volume filled with tissue. Both random and aligned fiber conduits had significantly more host tissue than film conduits at 4 weeks ($P < 0.05$). No significant differences were observed at 1 or 2 weeks following implantation (Fig. 3D).

In a third independent experiment, the site of injury was re-exposed at 4 weeks in six animals that received aligned fiber grafts. Upon re-exposure, we noted that the grafts retained their original placement and maintained good apposition to the rostral and caudal spinal cord stumps. Opening the grafts by a midline longitudinal incision on the dorsal surface revealed a large diameter tissue cable containing thin and dispersed blood vessels that had formed between the rostral and caudal stumps (Supplementary Movie). Staining of horizontal cryostat sections for rat endothelial cell antigen (RECA-1) demonstrated the presence of blood vessels at the immediate graft–cord interface at 1 week (Fig. 4A) and up to the center of the graft at 4 weeks (Fig. 4B). Laminin staining for basement membrane showed extensive vasculature at both the rostral and caudal spinal cord 4 weeks after injury (Fig. 4C), although the distribution of blood vessels differed between stumps in both random and aligned fiber groups (Fig. 4C–E shows an example from the random fiber group). The rostral stump contained blood vessels delineating the edge of the growth response (Fig. 4C,D), whereas blood vessels were abundant and disperse throughout the caudal stump (Fig. 4E).

3.3. Axonal regeneration

Horizontal sections were immunolabeled for neurofilament (RT97) and serotonin (5HT) to examine axonal regeneration after complete spinal cord transection. Neurofilament section overviews (Fig. 5A–J) demonstrated robust rostrocaudal axonal regeneration into aligned fiber conduits. One week after implantation, all groups displayed a similar pattern of RT97 staining (Fig. 5A–C). However, by 2 weeks neurofilament staining demonstrated robust rostrocaudal growth into aligned fiber conduits (Fig. 5F) that further elongated by 4 weeks (Fig. 5I). This response was observed exclusively from the rostral spinal cord. Interestingly, the regenerating axons inside aligned fiber conduits were remarkably linear (Fig. 5J). In random fiber conduits, individual RT97$^+$ axons entered the grafts at 2 weeks (Fig. 5E), and a modest rostrocaudal response was observed by 4 weeks (Fig. 5H). In film conduits, very few axons were present at the interface at 2 weeks (Fig. 5D), and at 4 weeks sparse RT97$^+$ axons were seen inside thin tissue strands (Fig. 5G). Axonal regeneration was quantified by measuring the distance between the rostral edge of the conduit to the 'axonal front', defined as the point of 10 or more contiguous axons [38]. Markedly, over 4 weeks, aligned fiber conduits promoted long distance axonal regeneration (2055 ± 150 μm), significantly greater than random fiber (1162 ± 87 μm) and film (413 ± 199 μm) conduits (Fig. 5M). At 4 weeks, all 7 animals from the aligned fiber group had robust regeneration present 1.5 mm from the rostral edge of the conduit compared with 1 animal from the random and 0 from the film groups (Fig. 5N). Serotonin staining revealed a considerable number of raphespinal (5HT$^+$) axons within the regeneration response (Fig. 5K). Retrograde tracing was used to identify neurons that regenerated axons inside conduits in 6 additional rats that received aligned fiber grafts. The goal of these tracing experiments was not to obtain a quantitative or descriptive comparison between aligned, random, and film conduits, but rather to identify the populations of supraspinal neurons contributing to the regeneration response observed in aligned conduits. Fast blue was injected in the center of the tissue cable present inside the graft 4 weeks after implantation. Fast blue positive neurons were identified in the spinal cord rostral to the conduit as well as in the raphe nuclei (64.5 ± 54.7), reticular formation (175.5 ± 105.9), red nucleus (68 ± 83), and the vestibular nuclei (28.5 ± 26.5).

At 4 weeks, 5HT$^+$ axons were present approximately 1 mm caudal to the graft in 3/21 animals (2 random, 1 aligned fiber) (Fig. 5L). It is important to note that 5HT$^+$ fibers undergo Wallerian degeneration after complete transection spinal cord injury, and by day 14 only a few fibers (<1%) remain scattered chiefly in the lumbar cord [39]. Our observations are consistent with the findings of Cheng and Olson [39] in that a few aberrant, residual 5HT$^+$ fibers are present in the lumbar cord at 2 weeks following injury. Cheng and Olson [39] also reported that at 21 days after injury almost all 5HT$^+$ fibers in the caudal cord have disappeared and no fibers can be found 30 days after complete transection injury. However, other groups report that serotoninergic interneurons may account for observations of 5HT$^+$ axons caudal to a complete transection injury [40]. No differences were detected in hindlimb function using the scale developed by Basso, Beattie, and Bresnahan (Supplementary Fig. 4) [36,37]. Although a few serotoninergic axons were observed caudal to the graft, the lack of 5HT$^+$ axons in the lumbar cord is in accordance with a lack of functional recovery up to 4 weeks after injury.

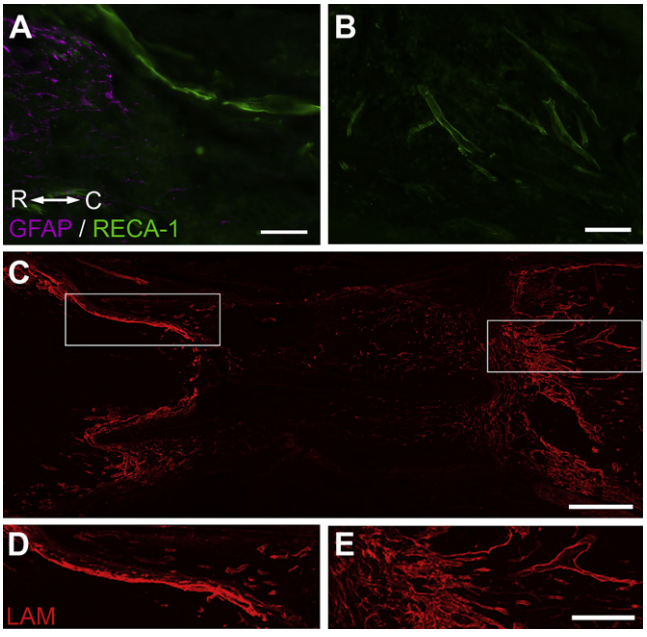

Fig. 4. Grafts support angiogenesis and are well vascularized 4 weeks following conduit implantation. Blood vessels are observed, by immunostaining for rat endothelial cell antigen 1 (RECA-1), at the rostral cord interface 1 week after implantation (A), and in the center of the graft at 4 weeks (B). C, Immunostaining for laminin in the basement membrane of blood vessels. A distinct difference in the pattern of vascularization is observed between the rostral (D) and caudal (E) spinal cord. In the rostral spinal cord, blood vessel formation occurs in close proximity to the regeneration front. D, E, Insets from (C). Scale bars: A, 100 μm; B, 50 μm; C, 500 μm; D, E, 200 μm.

3.4. Astrocytic response

Areas void of astrocytes were observed at the rostral cord in animals that received film conduits (Fig. 6A,D,G). Conversely, migration of astrocytes was observed in the rostrocaudal direction for random (Fig. 6B,E,H) and aligned (Fig. 6C,F,I) fiber conduits to an extent similar to the axonal growth. In the caudal stump, areas void of astrocytes were observed in all animals (Fig. 6A–I). Double-labeling for GFAP and RT97 indicated that the robust axonal

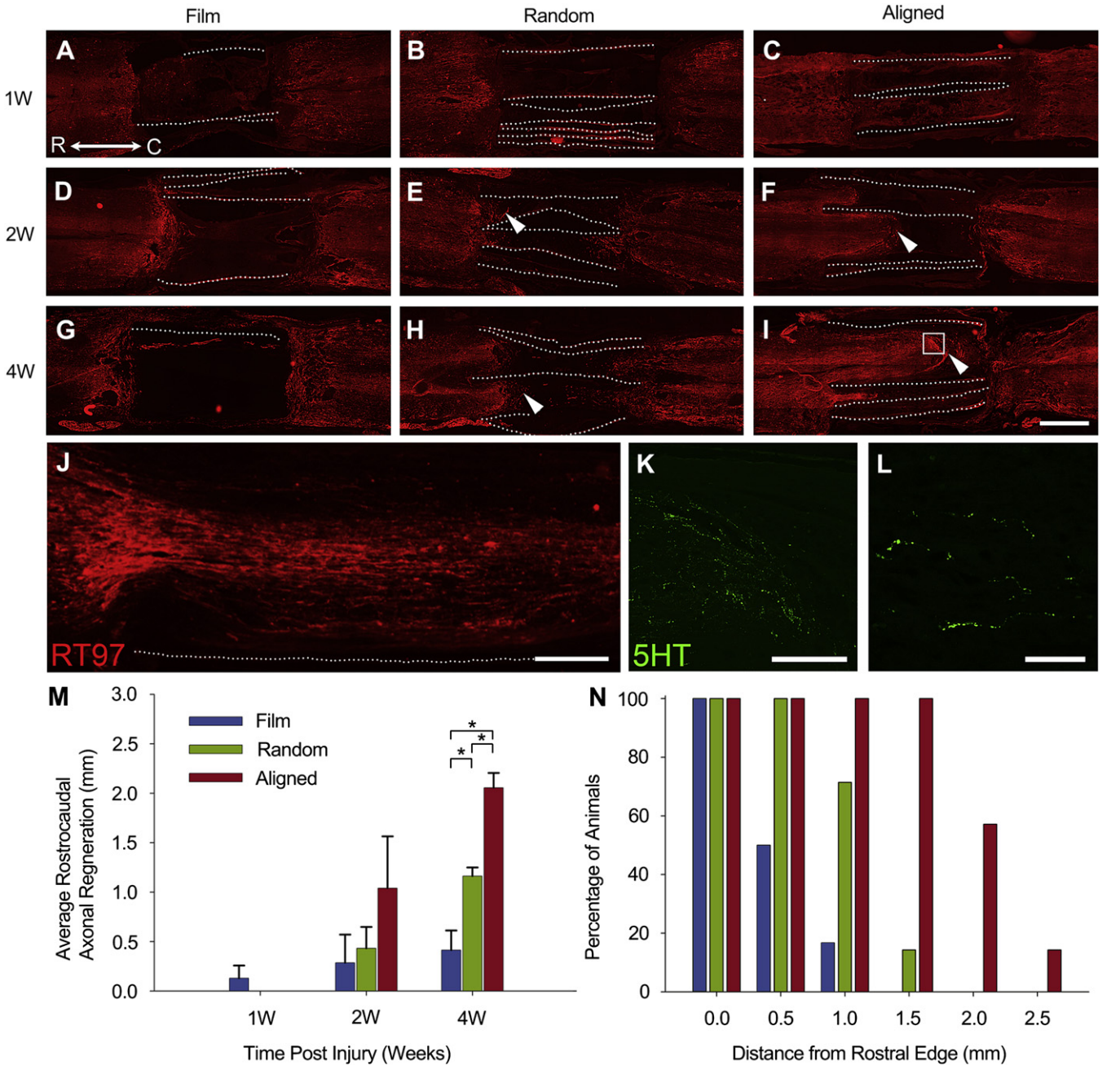

Fig. 5. Aligned fibers promote extensive axonal regeneration. Immunostaining for neurofilament (RT97) was used to visualize axons. Representative horizontal spinal cord sections for film (A, D, G), random (B, E, H), and aligned fiber (C, F, I) conduits. Aligned fibers foster robust, time dependent rostrocaudal axonal regeneration (C, F, I), whereas the same response is absent in film and random fiber conduits. Dotted lines indicate the walls of the conduits. Arrowheads (E, F, H, I) indicate the regeneration front. J, The axonal regeneration response inside aligned conduits was markedly linear, shown here in a different animal than that presented in (I). Serotonergic ($5HT^+$) axons were abundant in the robust growth observed inside aligned conduits (K, inset from adjacent section of the same animal in I). L, Serotonergic axons were present caudal to the graft in 3/21 animals (2 random, 1 aligned fiber). The distance between the rostral edge of the conduit to the 'axonal front' was quantified at all time points (M). Remarkably, over 4 weeks, aligned fibers promote robust, long distance regeneration (2055 ± 150 μm), significantly greater than random fiber (1162 ± 87 μm) and film (413 ± 199 μm) controls. Notably, at 4 weeks, 100% (7/7) of the animals from the aligned fiber group had a robust regeneration response present in the middle of the conduit compared to 14.3% (1/7) and 0% (0/6) in the random fiber and film groups, respectively (N). Data are mean ± SEM; $n = 3$ (1W, 2W), $n = 6–7$ (4W). *$P < 0.05$ by ANOVA. Scale bars: A-I, 1 mm; J, 500 μm; K, 150 μm; L, 50 μm.

regeneration response observed in aligned fiber conduits occurred in close proximity with astrocytes (Fig. 6J). High-resolution confocal imaging showed morphologically aligned astrocytes in close proximity to regenerating axons in aligned fiber conduits (Fig. 6K,L). We explored whether cultured astrocytes respond to the underlying topography (Fig. 7A–C), and exhibit a differential ability to migrate over each substrate (Fig. 7D–M). Interestingly, astrocytes exhibited a linear morphology when cultured on aligned fibers (Fig. 7C) in contrast to astrocytes cultured on film (Fig. 7A) or random fibers (Fig. 7B). Additionally, astrocytes migrate in a direction parallel to the median fiber orientation on aligned fibers, whereas astrocytes on random fibers were relatively static (Fig. 7D–M). The observation that migration on aligned fibers occurs only along the axis of the fibers indicates that differences in migration patterns both in vitro and in vivo are primarily a result of contact inhibition exerted by topography.

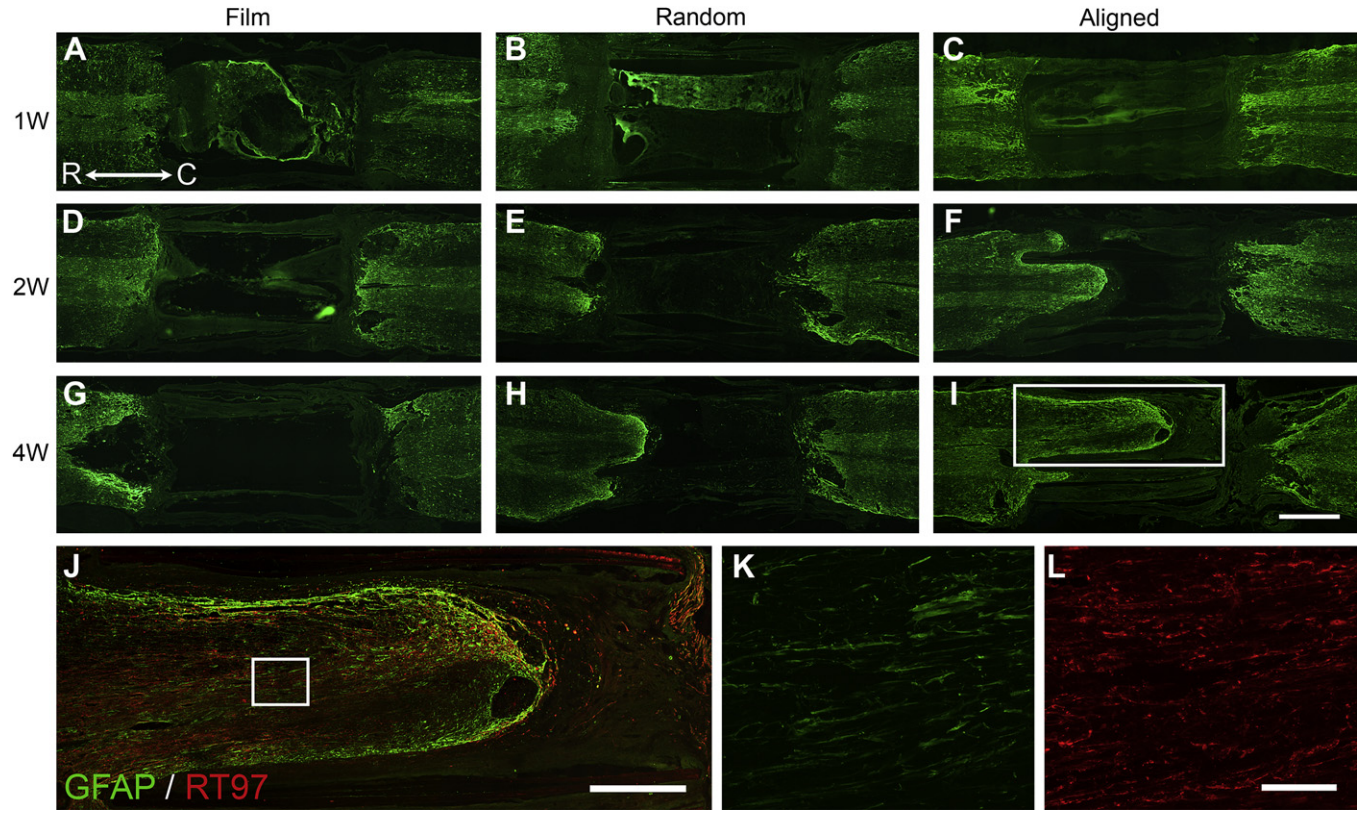

Fig. 6. Axonal regeneration is localized to migratory astrocytes. GFAP staining was used to visualize astrocytes. Representative horizontal spinal cord sections for film (A, D, G), random (B, E, H), and aligned fiber (C, F, I) conduits. Both random and aligned fibers support a time dependent migratory response of astrocytes (B, C, E, F, H, I), whereas time-dependent astrocytic dieback is observed in film conduits (D, G). Double-labeling for GFAP and RT97 indicates axonal regeneration is localized to astrocytes migrating from the rostral spinal cord (J, inset from I). High-magnification confocal micrographs show morphologically aligned migrating astrocytes in close proximity to regenerating axons (K and L, inset from J). Scale bars: A-I, 1 mm; J, 500 μm; K, L, 50 μm.

In order to assess the contribution of astrocytes to the axonal regeneration response, it was important to determine one of three alternatives: (1) astrocytes migrate into the conduit ahead of axons; (2) axons regenerate ahead of astrocytes; or (3) astrocytes and axons travel together. By examining the regeneration front in sections labeled for GFAP and RT97, we observed a number of leading pioneer axons in front of the bulk response at 4 weeks (Fig. 8B,C,E,F). This observation was pervasive in all animals with a robust response from the rostral spinal cord. In adjacent cresyl violet sections, bright field microscopy revealed the presence of polymer fibers that detached from the wall of random (Fig. 8A) and aligned fiber (Fig. 8D) conduits. These fibers were located ahead of the bulk tissue response matching the distribution of pioneer axons. To explore this result in further detail we examined in vitro axon growth and astrocyte migration from cortical explants (Fig. 9). Axon growth from cortical explants occurred in a similar manner to that of DRG explants; cortical neurons project axons on aligned fiber substrates in the direction of the underlying fibers (Fig. 9C; compare with Fig. 2C) whereas axons are projected without preferential direction on film or random fiber substrates (Fig. 9A,B; compare with Fig. 2A,B). Interestingly, as observed in vivo, the front of axonal growth from cortical explants is ahead of astrocyte migration (Fig. 9D–F).

4. Discussion

Spontaneous axonal regeneration after spinal cord injury is limited [1,2]. Traditional repair strategies have been successful in eliciting long distance regeneration of isolated axons. These approaches generally incorporate one or more components used to enhance regeneration, including potent promoters of neurite growth (NGF, NT-3, GDNF, BDNF, laminin) and growth permissive cells (i.e., Schwann cells, olfactory ensheathing glia) [7–9,15–25]. In this study, we developed an aligned microfiber-based synthetic polymer substratum that promoted robust CNS tissue growth without neurotrophin administration or cell transplants. We observed long distance (2055 ± 150 μm) axonal regeneration supported by migrating astrocytes. This response was remarkably similar to successful modes of PNS regeneration where axons are accompanied by supporting glia [30,31]. To the best of our knowledge, this form of CNS regeneration has not been reported.

In this study, we observed robust growth exclusively from the rostral spinal cord. We are certain that this response is indeed regeneration of host tissue. Mechanical effects (i.e. spinal cord/graft movement) cannot explain the outcome for several reasons. Up to 2 mm of spinal cord tissue was surgically removed to guarantee a 3 mm gap (Supplementary Fig. 1). Other groups that reported caudal migration of the rostral stump [41] did not remove tissue, relying on a gap created by a single complete transection. This gap may shorten immediately after surgery, leading to potential misinterpretation of results from late time points. To avoid graft migration, our conduits were fabricated to include a middle insert (Fig. 1F,N) that presents a mechanical barrier to movement; if rostral graft migration explains the rostrocaudal response, a 3 mm gap would have been present at a more caudal location. Moreover, these abovementioned mechanical factors would manifest early after injury/implantation. One week after implantation we did not observe this response. Additionally, a number of experimental

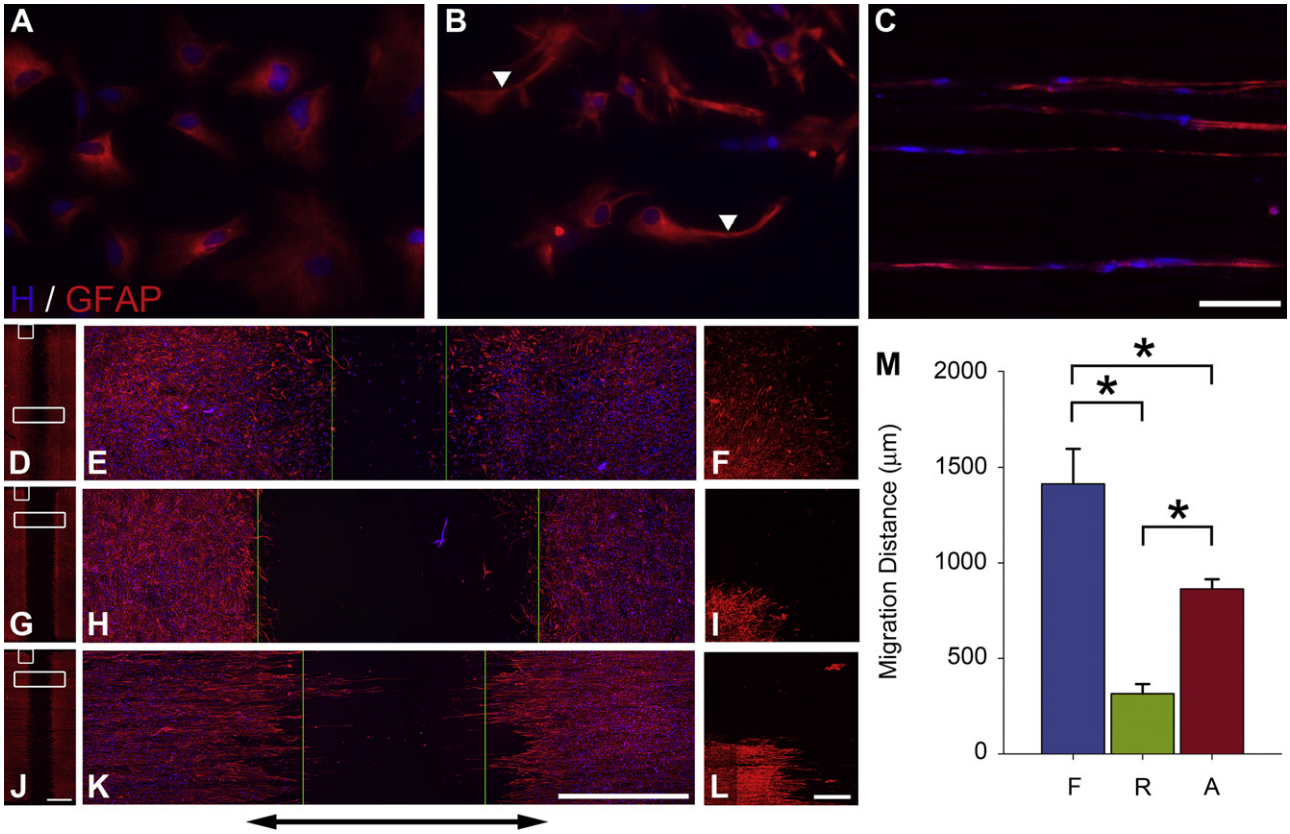

Fig. 7. Astrocytes exhibit morphological sensitivity to topographic cues and migrate in a topography dependent manner. Astrocytes isolated from embryonic rat cortices were cultured for 48 h on film (A), random (B), and aligned fiber (C) substrates. Arrows indicate close apposition of astrocytes to underlying polymer fibers in (B). Astrocytes exhibited a linear morphology when cultured on aligned fibers (C). In a migration assay (D–L), astrocytes cultured on film (D-F) and aligned fibers (J-L) partially close the initial 2.25 mm gap (indicated by black arrow), whereas astrocytes cultured on random fibers (G-I) remain relatively static over 5 days in culture (E, F, insets from D; H, I, insets from G; K, L, insets from J). Green lines in E, H, and K indicate the migration fronts. Interestingly, astrocytes are only able to migrate on aligned fibers in a direction parallel to the median fiber orientation (L). Migration of astrocytes on film is significantly greater than migration of astrocytes on random and aligned fibers, and migration of astrocytes on aligned fibers is significantly greater than migration of astrocytes on random fibers (M). Data are mean ± SEM; $n = 10$. $^{*}P < 0.05$ by ANOVA. Scale bars: A-C, 100 μm; D, G, J, 2 mm; E, F, H, I, K, L, 1 mm.

considerations support our interpretation. First, the robust rostrocaudal response was time dependent and therefore indicative of regeneration. One week after injury, no differences were observed (Fig. 5A–C and Fig. 6A–C). By two weeks, a difference in CNS tissue growth in the aligned fiber group was apparent and became significant by 4 weeks (Figs. 3,5, and 6). Second, the response was group-specific. At 4 weeks, 7/7 animals in the aligned fiber group had a robust regeneration response 1.5 mm into the conduit, whereas no animals from the film group had this response at the same distance (Fig. 5N). Third, the data from the 4 week time point was collected over two independent experiments and results were consistent between experiments. In a third independent experiment, conduits were re-exposed at 4 weeks in 6 animals that received aligned fiber grafts. The grafts for each of the 6 animals retained their original placement, and conduits contained a large diameter tissue cable within their lumen, continuous with the rostral and caudal spinal cord stumps (Supplementary Movie). Thus the simplest interpretation and the most significant result of our findings is that the rostrocaudal response is true regeneration of host neural tissue.

In our model we observed long distance regeneration of individual axons, similar to that demonstrated by other groups [21–23,25]. An important distinction between this work and that of others is that isolated pioneering axons are followed by bulk regeneration of axons accompanied by astrocytes (Fig. 6J–L and Fig. 8B,C,E,F). While the role of astrocytes in spinal cord repair is contentious, here the close apposition of astrocytes to regenerating axons suggests a supportive role. Other groups have demonstrated that astrocyte associated fibronectin is critical for axonal regeneration [42], and astrocytes can protect neurons from immune-mediated secondary injury [43]. Although astrocytes supported bulk regeneration of axons, we found isolated pioneer axons leading the response. This response is reminiscent of staggered corticospinal tract development where pioneer axon growth precedes the bulk growth of fasciculating corticospinal axons [44,45]. In accordance with this observation, we found that axonal growth from cultured cortical explants is ahead of the astrocyte migration front (Fig. 9). A number of cells contributed to complete transection gap closure and integrated ahead of the regeneration response with polymer fibers that had detached from the conduit wall (Fig. 8A,D). Identification of cell populations and subsequent cellular mechanisms that led to this regeneration response will be the focus of future studies.

Aligned fiber conduits promoted significantly greater regeneration than the random fiber control (Fig. 5M). We attribute this difference to the ability of aligned fibers to promote efficient regeneration. In order to examine growth efficiency, we compared the growth of DRG neurites from explants cultured on aligned fibers to those from DRG cultured on film and random fiber substrates (Fig. 2). Consistent with previous reports [28–30,34,46], aligned fibers demonstrated an ability to guide growth of DRG neurites. Importantly, the contact guidance provided by aligned

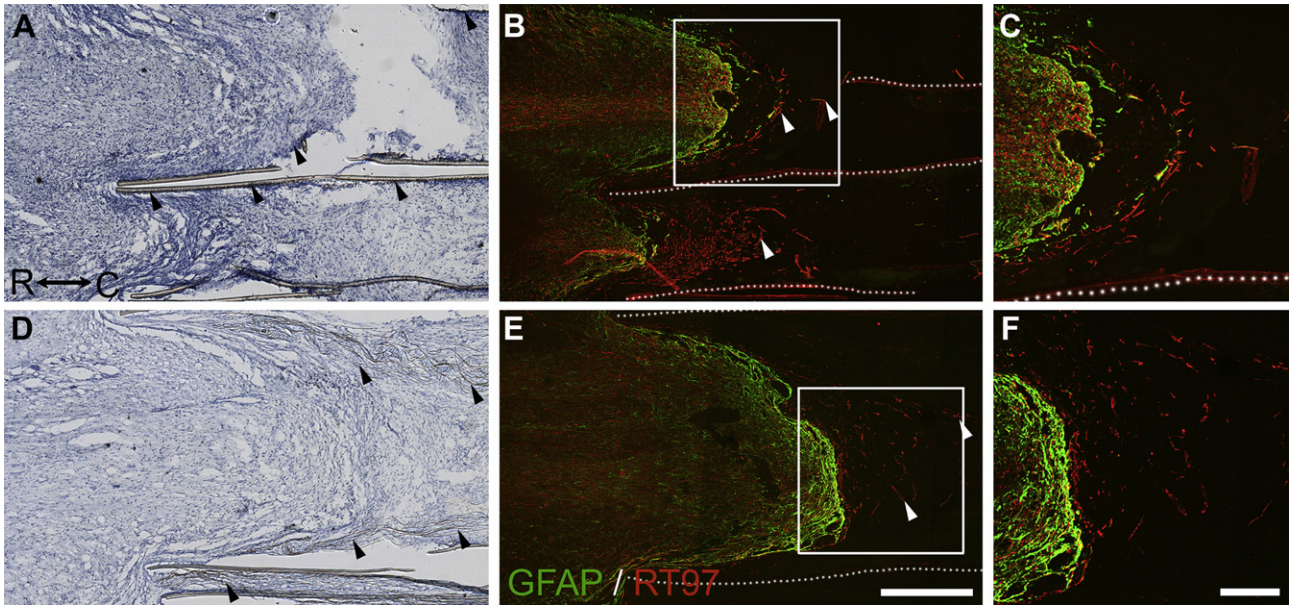

Fig. 8. Pioneer axons guide the regeneration response from the rostral spinal cord. A, D, Cresyl violet staining in sections adjacent to GFAP/RT97 stained sections (B, E) demonstrate that polymer fibers guide rostrocaudal growth in random (A) and aligned fiber (D) conduits. Black arrowheads point to polymer fibers; random fibers in (A) project orthogonal to the plane of the tissue section, whereas aligned fibers (D) remain in the plane of the section. B, E, After 4 weeks, astrocytes (GFAP) and regenerating axons (RT97) enter random (B) and aligned fiber (E) conduits in close proximity, and axons lead the response. Dotted lines indicate the walls of the conduits. White arrowheads point to axons at the regeneration front. C, Inset from (B). F, Inset from (E). Scale bars: B, E, 500 μm; C, F, 200 μm.

microfibers allowed neurites to reach longer distances (Fig. 2G,H), a desired characteristic for neural tissue repair. In an astrocyte migration assay, astrocytes migrate on aligned fiber substrates on the axis of fiber orientation, but not in the perpendicular direction (Fig. 7L). Additionally, astrocytes on random fibers remain relatively static over 5 days in culture (Fig. 7G–I). Together these data indicate that aligned fibers orient populations of migrating cells through contact inhibition. Other groups have used aligned micro/nano fiber based conduits to bridge long (>15 mm in rats) peripheral nerve gaps [30,31]. Our results in the CNS are in accordance with those of others in the PNS showing that axon regeneration was enhanced in the longitudinally aligned fiber group over random [30] or circumferentially oriented fibers [31]. In the CNS, electrospun fibers have been used to deliver Rolipram after lateral spinal cord hemisection [47]. Our data substantiate this indication that electrospun fibers may enhance regeneration after spinal cord injury.

We do not understand why there is robust regeneration from the rostral, and not from the caudal, spinal cord. Plant et al. [48] suggested several potential contributors to rostral/caudal asymmetry, including (1) Wallerian degeneration of descending or ascending axons; (2) supraspinal versus propriospinal and afferent sensory axon capacity for regeneration; (3) incontiguous cerebrospinal fluid flow; (4) amount and character of angiogenesis in the graft and stumps; (5) number/activation state of infiltrating macrophages; and (6) astrocyte reactivity. An additional difference

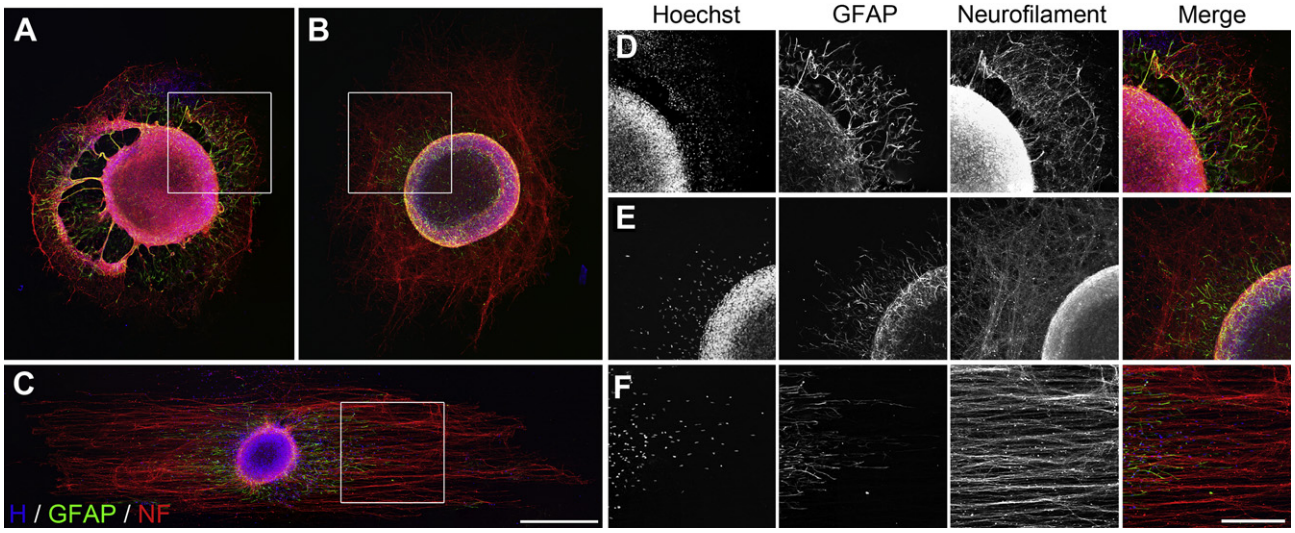

Fig. 9. Axon growth precedes astrocyte migration from cortical explants in vitro. Cortical explants were isolated from E18 rat pups and cultured on film (A), random (B), and aligned (C) fiber substrates for 5 days. D, E, F, Insets of astrocyte migration fronts from cortical explants (D, inset from A; E, inset from B; F, inset from C) demonstrate that axonal growth from cortical explants is ahead of astrocyte migration. Scale bars: A-C, 500 μm; D-F, 250 μm.

intrinsic to a complete transection is the deprivation of supraspinal innervation to the caudal stump. In the present study we observed a dense matrix at the caudal stump as early as 1 week post injury (Supplementary Fig. 3C). Although in other studies a similar matrix forms at the rostral edge of the graft [22,23], we did not observe this effect in random or aligned fiber conduits (Fig. 3B,C). Another clear difference between spinal cord stumps was the astrocytic dieback observed in the distal stump in all groups. Additionally, we observed differences in the character of blood vessel distribution between the rostral and caudal stumps (Fig. 4C). Blood vessels encompass the regeneration response at the rostral edge of the conduit (Fig. 4D), whereas the extensive vascularization at the caudal interface appears disorganized (Fig. 4E).

5. Conclusion

Although long distance axonal regeneration in the CNS was previously thought to occur only in the presence of growth permissive biological substrates, we demonstrate the ability of adult CNS tissue to regenerate extensively without administration of cells, neurotrophins, antibodies, enzymes, or chemical compounds. Grafts containing aligned PLA microfibers promote regeneration of CNS tissue composed of regenerating axons from supraspinal and propriospinal neurons accompanied by glial cells. Indeed, this robust growth represents a novel mode of CNS regeneration, and future studies focusing on understanding mechanisms contributing to this response will lead to insights in regeneration biology and molecular targets for intervention after spinal cord injury.

Acknowledgments

This work was supported by the Kennedy Krieger Institute, and the National Institutes of Health—National Institute of Neurological Disorders and Stroke Grant R21NS62392 (R.J.G.) and National Institute of Child Health and Human Development Grant R15HD61096 (R.J.G.). The Animal Injury and Repair Core laboratory at the International Center for Spinal Cord Injury cared for all animals and performed behavioral testing. The authors would like to thank Dr. Devin S. Gary for providing technical assistance with astrocyte culture, Misty Malone for providing DRG explants, and David Rini for the production of artwork/drawings. The authors are grateful to Dr. Frank Bradke, Dr. Ronald Schnaar, and Dr. Lawrence Schramm for their critical evaluation of the manuscript. The RT97 monoclonal antibody developed by J. Wood was obtained from the Developmental Studies Hybridoma Bank developed under the auspices of the NICHD and maintained by The University of Iowa, Department of Biology, Iowa City, IA 52242.

Appendix. Supplementary material

Supplementary data associated with this article can be found, in the online version, at doi:10.1016/j.biomaterials.2011.05.006.

References

[1] Silver J, Miller JH. Regeneration beyond the glial scar. Nat Rev Neurosci 2004; 5:146–56.
[2] Ylera B, Ertürk A, Hellal F, Nadrigny F, Hurtado A, Tahirovic S, et al. Chronically CNS-injured adult sensory neurons gain regenerative competence upon a lesion of their peripheral axon. Curr Biol 2009;19:930–6.
[3] Hellal F, Hurtado A, Ruschel J, Flynn KC, Laskowski CJ, Umlauf M, et al. Microtubule stabilization reduces scarring and causes axon regeneration after spinal cord injury. Science 2011;331:928–31.
[4] Moore DL, Blackmore MG, Hu Y, Kaestner KH, Bixby JL, Lemmon VP, et al. KLF family members regulate intrinsic axon regeneration ability. Science 2009; 326:298–301.
[5] Neumann S, Bradke F, Tessier-Lavigne M, Basbaum AI. Regeneration of sensory axons within the injured spinal cord induced by intraganglionic cAMP elevation. Neuron 2002;34:885–93.
[6] Qiu J, Cai D, Dai H, McAtee M, Hoffman PN, Bregman BS, et al. Spinal axon regeneration induced by elevation of cyclic AMP. Neuron 2002;34:895–903.
[7] Pearse DD, Pereira FC, Marcillo AE, Bates ML, Berrocal YA, Filbin MT, et al. cAMP and Schwann cells promote axonal growth and functional recovery after spinal cord injury. Nat Med 2004;10:610–6.
[8] Tuszynski MH, Gage FH. Bridging grafts and transient nerve growth factor infusions promote long-term central nervous system neuronal rescue and partial functional recovery. Proc Natl Acad Sci USA 1995;92:4621–5.
[9] Oudega M, Hagg T. Nerve growth factor promotes regeneration of sensory axons into adult rat spinal cord. Exp Neurol 1996;140:218–29.
[10] Schnell L, Schwab ME. Axonal regeneration in the rat spinal cord produced by an antibody against myelin-associated neurite growth inhibitors. Nature 1990;343:269–72.
[11] Chen MS, Huber AB, van der Haar ME, Frank M, Schnell L, Spillmann AA, et al. Nogo-A is a myelin-associated neurite outgrowth inhibitor and an antigen for monoclonal antibody IN-1. Nature 2000;403:434–9.
[12] Yang LJS, Lorenzini I, Vajn K, Mountney A, Schramm LP, Schnaar RL. Sialidase enhances spinal axon outgrowth in vivo. Proc Natl Acad Sci USA 2006;103: 11057–62.
[13] Bradbury EJ, Moon LDF, Popat RJ, King VR, Bennett GS, Patel PN, et al. Chondroitinase ABC promotes functional recovery after spinal cord injury. Nature 2002;416:636–40.
[14] Hurtado A, Podinin H, Oudega M, Grimpe B. Deoxyribozyme-mediated knockdown of xylosyltransferase-1 mRNA promotes axon growth in the adult rat spinal cord. Brain 2008;131:2596–605.
[15] Richardson PM, McGuinness UM, Aguayo AJ. Axons from CNS neurons regenerate into PNS grafts. Nature 1980;284:264–5.
[16] David S, Aguayo AJ. Axonal elongation into peripheral nervous system "bridges" after central nervous system injury in adult rats. Science 1981;214: 931–3.
[17] Houle JD, Tom VJ, Mayes D, Wagoner G, Phillips N, Silver J. Combining an autologous peripheral nervous system "bridge" and matrix modification by chondroitinase allows robust, functional regeneration beyond a hemisection lesion of the adult rat spinal cord. J Neurosci 2006;26:7405–15.
[18] Tom VJ, Sandrow-Feinberg HR, Miller K, Santi L, Conners T, Lemay M, et al. Combining peripheral nerve grafts and chondroitinase promotes functional axonal regeneration in the chronically injured spinal cord. J Neurosci 2009;29: 14881–90.
[19] Berry M, Rees L, Hall S, Yiu P, Sievers J. Optic axons regenerate into sciatic nerve isografts only in the presence of Schwann cells. Brain Res Bull 1988;20: 223–31.
[20] Berry M, Hall S, Follows R, Rees L, Gregson N, Sievers J. Response of axons and glia at the site of anastomosis between the optic nerve and cellular or acellular sciatic nerve grafts. J Neurocytol 1988;17:727–44.
[21] Xu XM, Guénard V, Kleitman N, Aebischer P, Bunge MB. A combination of BDNF and NT-3 promotes supraspinal axonal regeneration into Schwann cell grafts in adult rat thoracic spinal cord. Exp Neurol 1995;134:261–72.
[22] Xu XM, Guénard V, Kleitman N, Bunge MB. Axonal regeneration into Schwann cell-seeded guidance channels grafted into transected adult rat spinal cord. J Comp Neurol 1995;351:145–60.
[23] Coumans JV, Lin TTS, Dai HN, MacArthur L, McAtee M, Nash C, et al. Axonal regeneration and functional recovery after complete spinal cord transection in rats by delayed treatment with transplants and neurotrophins. J Neurosci 2001;21:9334–44.
[24] Hurtado A, Moon LDF, Maquet V, Blits B, Jérôme R, Oudega M. Poly (D,L-lactic acid) macroporous guidance scaffolds seeded with Schwann cells genetically modified to secrete a bi-functional neurotrophin implanted in the completely transected adult rat thoracic spinal cord. Biomaterials 2006;27: 430–42.
[25] Stokols S, Tuszynski MH. Freeze-dried agarose scaffolds with uniaxial channels stimulate and guide linear axonal growth following spinal cord injury. Biomaterials 2006;27:443–51.
[26] Lu P, Tuszynski MH. Growth factors and combinatorial therapies for CNS regeneration. Exp Neurol 2008;209:313–20.
[27] Quencer R, Bunge RP. The injured spinal cord: imaging, histopathologic, clinical correlates, and basic science approaches to enhancing neural function after spinal cord injury. Spine 1996;21:2064–6.
[28] Wang HB, Mullins ME, Cregg JM, Hurtado A, Oudega M, Trombley MT, et al. Creation of highly aligned electrospun poly-L-lactic acid fibers for nerve regeneration applications. J Neural Eng 2009;6:016001.
[29] Corey JM, Lin DY, Mycek KB, Chen Q, Samuel S, Feldman EL, et al. Aligned electrospun nanofibers specify the direction of dorsal root ganglia neurite growth. J Biomed Mater Res A 2007;83:636–45.
[30] Kim YT, Haftel VK, Kumar S, Bellamkonda RV. The role of aligned polymer fiber-based constructs in the bridging of long peripheral nerve gaps. Biomaterials 2008;29:3117–27.
[31] Chew SY, Mi R, Hoke A, Leong KW. Aligned protein-polymer composite fibers enhance nerve regeneration: a potential tissue-engineering platform. Adv Funct Mater 2007;17:1288–96.
[32] Clements IP, Kim YT, English AW, Lu X, Chung A, Bellamkonda RV. Thin-film enhanced nerve guidance channels for peripheral nerve repair. Biomaterials 2009;30:3834–46.

[33] Smith GM, Strunz C. Growth factor and cytokine regulation of chondroitin sulfate proteoglycans by astrocytes. Glia 2005;52:209–18.
[34] Xie J, MacEwan MR, Li X, Sakiyama-Elbert SE, Xia Y. Neurite outgrowth on nanofiber scaffolds with different orders, structures, and surface properties. ACS Nano 2009;3:1151–9.
[35] Xie J, Willerth SM, Li X, Macewan MR, Rader A, Sakiyama-Elbert SE, et al. The differentiation of embryonic stem cells seeded on electrospun nanofibers into neural lineages. Biomaterials 2009;30:354–62.
[36] Basso DM, Beattie MS, Bresnahan JC. A sensitive and reliable locomotor rating scale for open field testing in rats. J Neurotrauma 1995;12:1–21.
[37] Basso DM, Beattie MS, Bresnahan JC. Graded histological and locomotor outcomes after spinal cord contusion using the NYU weight-drop device versus transection. Exp Neurol 1996;139:244–56.
[38] Shen Y, Tenney AP, Busch SA, Horn KP, Cuascut FX, Liu K, et al. PTPσ is a receptor for chondroitin sulfate proteoglycan, an inhibitor of neural regeneration. Science 2009;326:592–6.
[39] Cheng H, Olson L. A new surgical technique that allows proximodistal regeneration of 5-HT fibers after complete transection of the rat spinal cord. Exp Neurol 1995;136:149–61.
[40] Takeoka A, Kubasak MD, Zhong H, Roy RR, Phelps PE. Serotonergic innervation of the caudal spinal stump in rats after complete spinal transection: effect of olfactory ensheathing glia. J Comp Neurol 2009;515:664–76.
[41] Nomura H, Katayama Y, Shoichet MS, Tator CH. Complete spinal cord transection treated by implantation of a reinforced synthetic hydrogel channel results in syringomyelia and caudal migration of the rostral stump. Neurosurgery 2006;58:183–92.
[42] Tom VJ, Doller CM, Malouf AT, Silver J. Astrocyte-associated fibronectin is critical for axonal regeneration in adult white matter. J Neurosci 2004;24:9282–90.
[43] Faulkner JR, Herrmann JE, Woo MJ, Tansey KE, Doan NB, Sofroniew MV. Reactive astrocytes protect tissue and preserve function after spinal cord injury. J Neurosci 2004;24:2143–55.
[44] Schreyer DJ, Jones EG. Growth and target finding by axons of the corticospinal tract in prenatal and postnatal rats. Neuroscience 1982;7:1837–53.
[45] Joosten EAJ. Developmental expression of N-CAM epitopes in the rat spinal cord during corticospinal tract axon outgrowth and target innervation. Dev Brain Res 1994;78:226–36.
[46] Wang HB, Mullins ME, Cregg JM, McCarthy CW, Gilbert RJ. Varying the diameter of aligned electrospun fibers alters neurite outgrowth and Schwann cell migration. Acta Biomater 2010;6:2970–8.
[47] Zhu Y, Wang A, Shen W, Patel S, Zhang R, Young WL, et al. Nanofibrous patches for spinal cord regeneration. Adv Funct Mater 2010;20:1–8.
[48] Plant GW, Bates ML, Bunge MB. Inhibitory proteoglycan immunoreactivity is higher at the caudal than the rostral Schwann cell graft-transected spinal cord interface. Mol Cell Neurosci 2001;17:471–87.